SUPPLEMENTARY INFORMATION

Extreme Downsizing of Spin Crossover Nanoparticles Towards Stable Colloids in Water: A Detailed Nano -Topographic Study

Christina D. Polyzou,*[a] Ondřej Malina,*[b] Michaela Polaskova,[b,c] Manoj Tripathi,[d] Alan B. Dalton,[d] John Parthenios[e] and Vassilis Tangoulis*[a]

[a] Department of Chemistry, Laboratory of Inorganic Chemistry, University of Patras, 26504, Patras, Greece. Email: chpolyzou@upatras.gr and vtango@upatras.gr

[b] Regional Centre of Advanced Technologies and Materials, Czech Advanced Technology and Research Institute (CATRIN), Palacký University Olomouc, Czech Republic. Email: ondrej.malina@upol.cz

[c] Department of Experimental Physics, Faculty of Sciences of the Czech Republic, v.v.i., Flemingovo nám. 2, 16610 Prague 6, Czech Republic

[d] Department of Physics and Astronomy, University of Sussex, Brighton BN1 9RH, U.K.

[e] Institute of Chemical Engineering Sciences, Foundation of Research and Technology-Hellas (FORTH/ICE-HT), Stadiou Street, Platani, Patras, 26504 Greece

Table of Contents

Synthetic comments. TEM microscopy

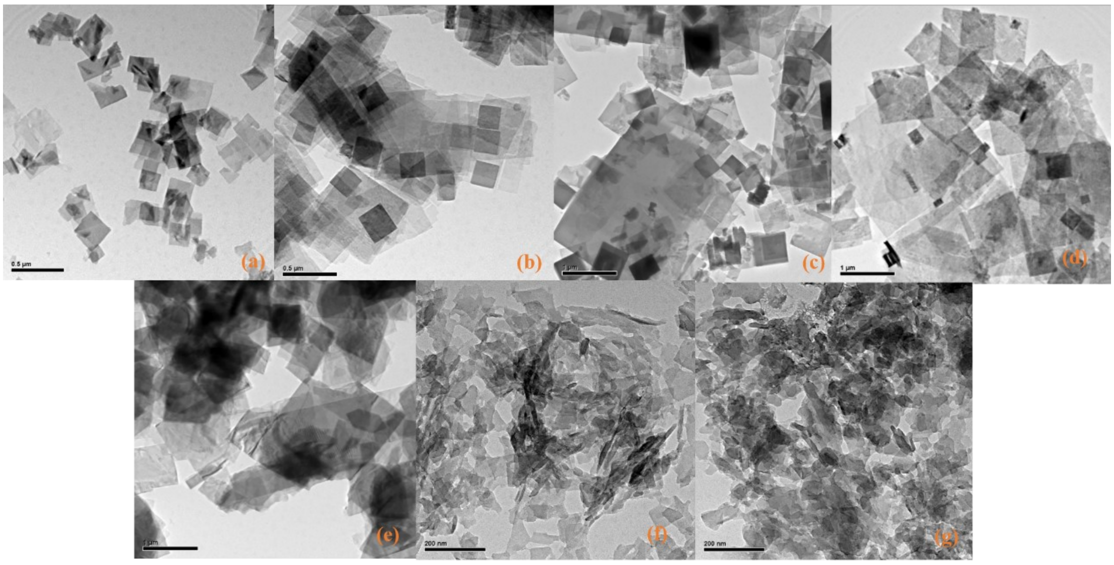

Fig. S1. TEM images from all the unsuccessful attempts of the synthesized nanoparticles showing their varying size and distribution.

Table S1. Size and distribution of synthesized nanoparticles in various reaction ratios and concentrations.

Size distribution	Reaction Ratio	Concentration	Fig.
100 nm - 500 nm	1:1:3	0.15 M	S1(a)
100 nm – 700 nm	1:1:3	0.13 M	S1(b)
100 nm – 2 µm	1:1:6	0.1 M	S1(c)
100 nm – 1 µm	1:1:3	0.1 M	S1(d)
400 nm – 1 µm	1:1:3	0.05 M	S1(e)
Indefinable size	1:1:10	0.1 M	S1(f)
Indefinable size	1:1:10	0.13 M	S1(g)

Elemental Analysis

Table S2. Elemental analyses for samples **1** - **6**.

Sample		**C** [%]	**N** [%]	**H** [%]	**Molecular Formulae**
1	exptl	**41.58**	**26.43**	**3.12**	$[Fe^{II}(2\text{-mpz})_2Ni(CN)_4]$
	calcd	41.38	27.59	2.98	406 g/mol
2	exptl	**42.55**	**27.50**	**3.28**	$[Fe^{II}(2\text{-mpz})_2Ni(CN)_4]\cdot(2\text{-mpz})_{0.2}$
	calcd	42.37	27.69	3.13	425 g/mol
3	exptl	**48.59**	**28.03**	**4.20**	$[Fe^{II}(2\text{-mpz})_2Ni(CN)_4]\cdot(2\text{-mpz})_2$
	calcd	48.48	28.28	4.07	594 g/mol
4	exptl	**42.91**	**28.92**	**3.78**	$[Fe^{II}(2\text{-mpz})_2Ni(CN)_4]\cdot(2\text{-mpz})_{0.8}$
	calcd	42.74	29.02	3.66	463 g/mol
5	exptl	**43.90**	**27.70**	**3.46**	$[Fe^{II}(2\text{-mpz})_2Ni(CN)_4]\cdot(2\text{-mpz})_{0.5}$
	calcd	43.71	27.82	3.34	453 g/mol
6	exptl	**42.54**	**27.53**	**3.26**	$[Fe^{II}(2\text{-mpz})_2Ni(CN)_4]\cdot(2\text{-mpz})_{0.2}$
	calcd	42.37	27.69	3.13	425 g/mol

TG Analysis

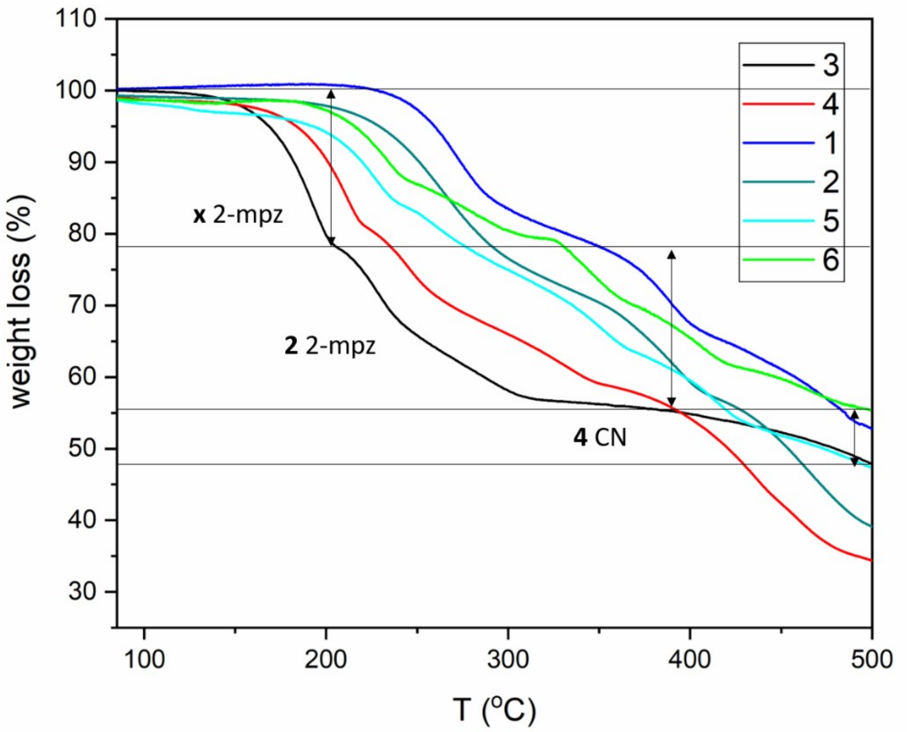

Fig. S2. TG analysis for compounds **1**, **2**, **3** and nanoparticle **4**, **5, 6** (degradation details for compound **3**).

TGA analysis for compounds **1** - **6** shows the gradual degradation of polymers in Fig. S13. Compound **1** seems to be free of water or 2-mpz molecules on the lattice, while samples **2** and **6** seem to host small percentages of 2-mpz molecules on their lattices. The three degradation steps are attributed to 2-mpz lattice molecules, the two coordinated 2-mpz ligands and the CN group. In case of compounds **3**, **4** and **5** the degradation begins in relative lower temperatures (between 100 and 120 ^{o}C) than the rest of compounds (between 150 and 220 ^{o}C). Besides, it is obvious that the degradation rate is greater in compound **3** than compounds **4** and **5** revealing the presence of greater percentage of 2-mpz lattice molecules. The latter conclusion is also confirmed by the presence of four degradation steps in **3**, **4** and **5** (1st for lattice 2-mpz, 2nd and 3rd for coordinated 2-mpz molecules and 4th for CN groups).

Crystallographic Description

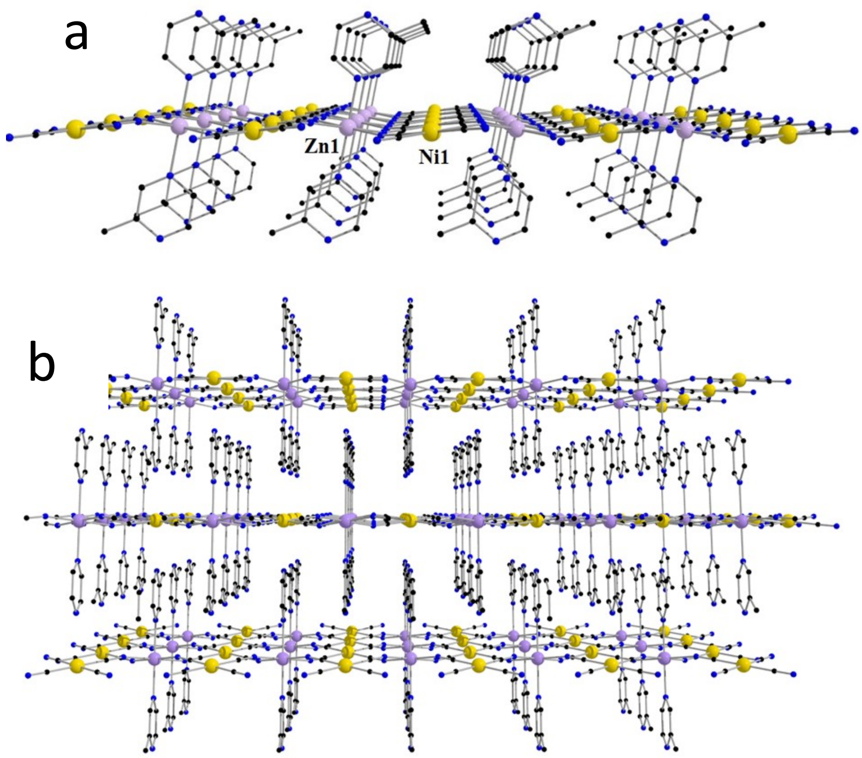

Figure S3. (a) View of the crystal structure of of the diamagnetic isotructural analogue [Zn^{II}(2-mpz)$_2$Ni(CN)$_4$] in the *ac* plane. (b) 2D-pillared interacting layers. H atoms are omitted for clarity [Zn: pale purple, Ni: yellow, C: black, N: blue].

AFM topography of nanoparticles **6**

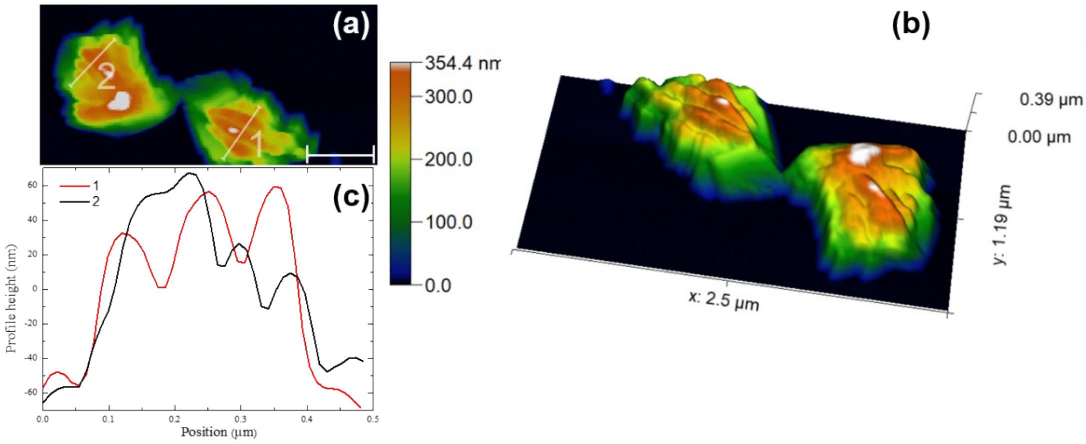

Fig. S4. (a) A two dimensional topography AFM imaging of two individual nanoparticles **6** (Scale bar: 500 nm), (b) the corresponding 3D representation of (a) and (c) the height profiles 1 and 2 shown in (a).

AFM topography of nanoparticles $\mathbf{6}_{exf}$

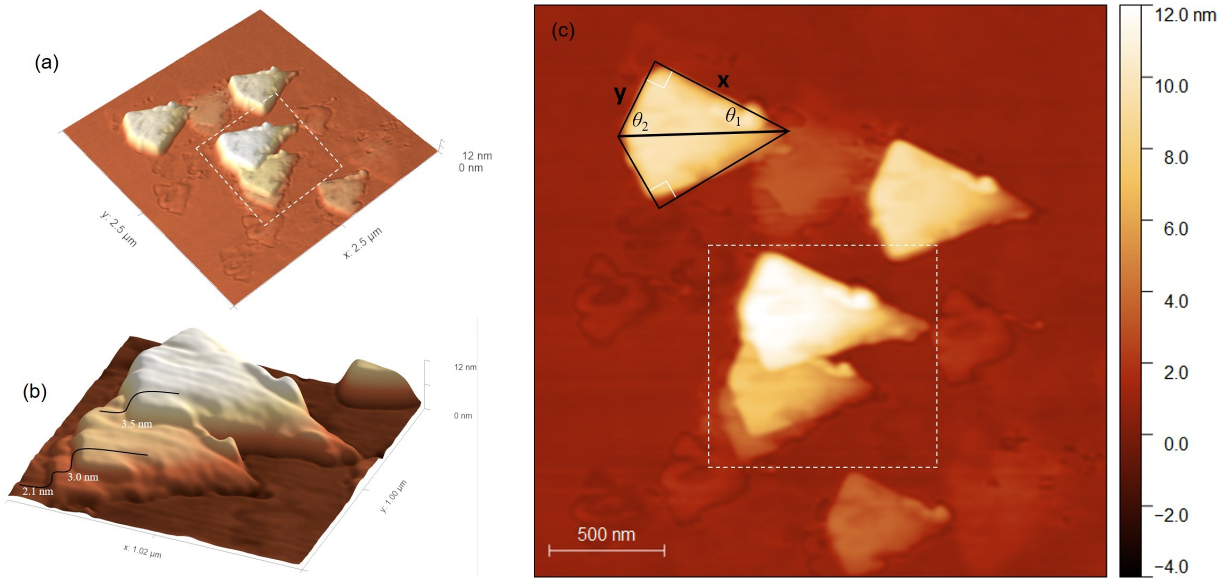

Fig. S5. (a) The 3D AFM topography of Fig. 3b showing a large number of individual nanoparticles of various thicknesses. (b) The 3D magnified region enclosed in the white dashed rectangle in Fig. S5a and (c) the AFM image of Fig. 3b showing the two right triangles that delineate the base face of the right prism. The characteristic triangle sides and angles are also shown. The area in the dashed line rectangle is magnified in Fig. S5b.

AFM topography of nanoparticles $\mathbf{6}_{exf}$

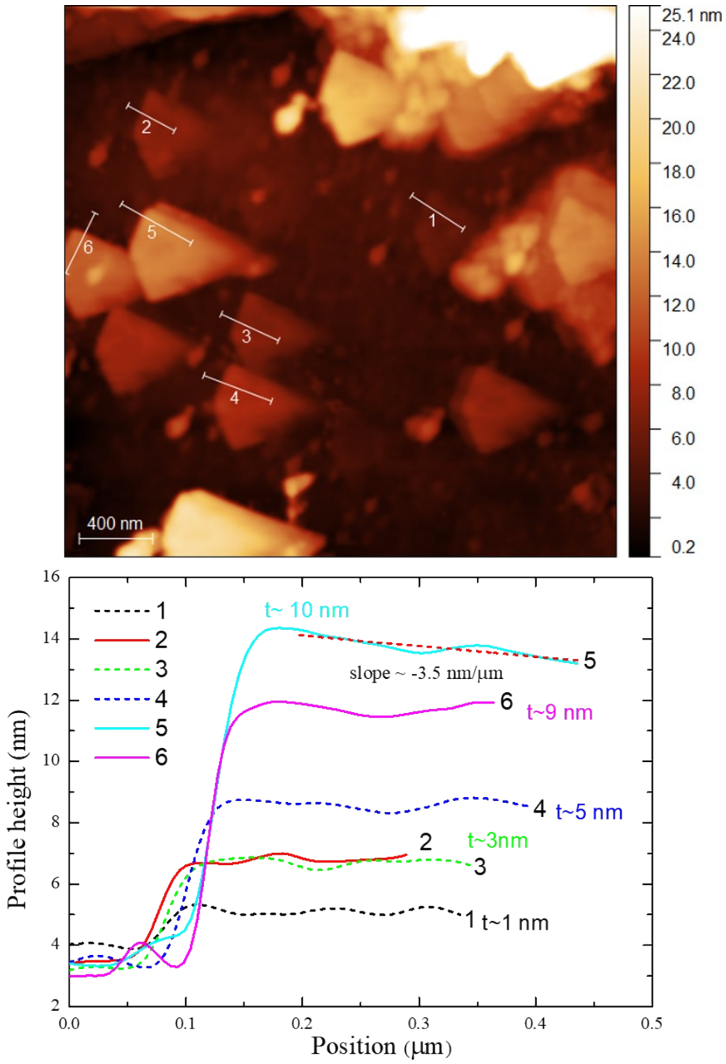

Fig. S6. Upper panel: a two dimensional AFM topography image showing individual nanoparticles. Lower panel: Height profiles corresponding to the solid lines AFM images, t is the thickness of each nanoparticle.

Calculation of triangle sides and angles of nanoparticles $\mathbf{6}_{exf}$

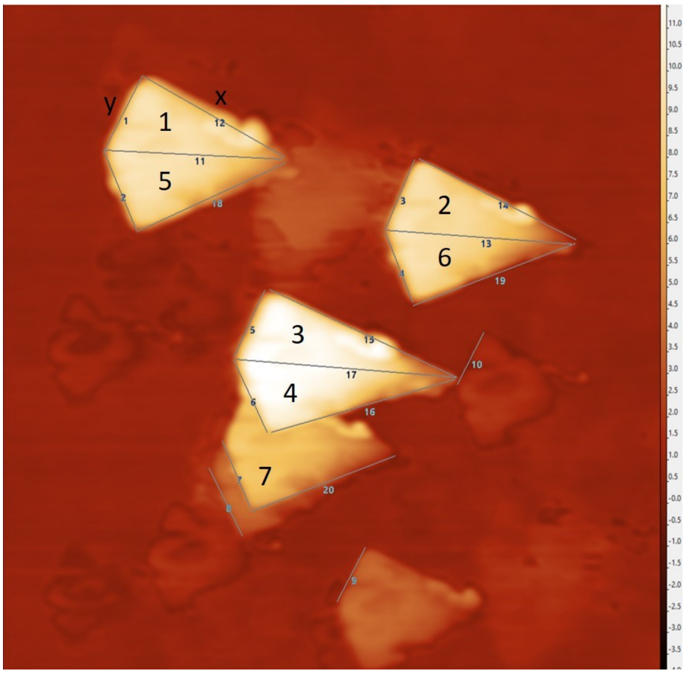

Fig. S7. AFM topography images of Fig. 3b showing the right triangles used for measuring the characteristic triangle sides and angles. The measurements are summarized in Table S3.

Area and volume calculations [1]

Area: $A = \frac{1}{2}(x^2 + y^2)sin\theta_2$

Volume:

$V = Ah$ right prism (inset in fig.1a, lower panel)

$V = 2A\frac{h_1 + h_2 + h_3}{3}$ where h1, h2 and h3 are the minimum, the intermediate and the maximum heights in a truncated right prism (inset in Fig. 1b, lower panel).

Table S3. The characteristic triangle sides and angles of nanoparticles of Fig. S7.

X (μm)	**y (μm)**	**hypotenuse (μm)**	**θ1**	**θ2**	**2*θ2**	**triangle #**
0.62	0.32	0.70	27.30	62.70	125.40	1
0.66	0.28	0.72	22.99	67.01	134.02	2
0.78	0.27	0.83	19.36	70.64	135.58	3
0.72	0.29	0.78	22.21	67.79		4
0.62	0.33	0.70	28.02	61.98	123.95	5
0.65	0.28	0.71	23.30	66.70	133.39	6
0.58	0.27	0.64	24.96	65.04	130.07	7
0.66 (7)	**0.29 (2)**	**0.72 (6)**	**24.02**	**66 (3)**	**132 (6)**	

[1] William F. Kern, James R Bland, *Solid Mensuration with proofs,* John Wiley & Sons New York 1947.

IR spectroscopy

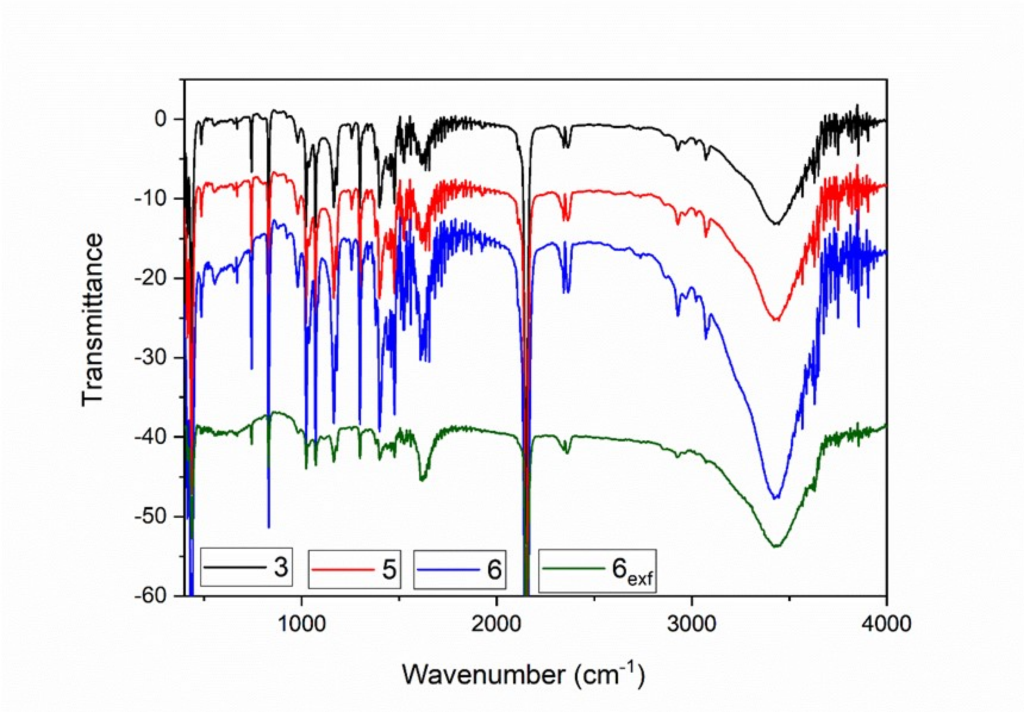

Fig. S8. IR spectra of compound **3** and nanoparticles **5**, **6** and **6$_{exf}$**.

pXRD patterns

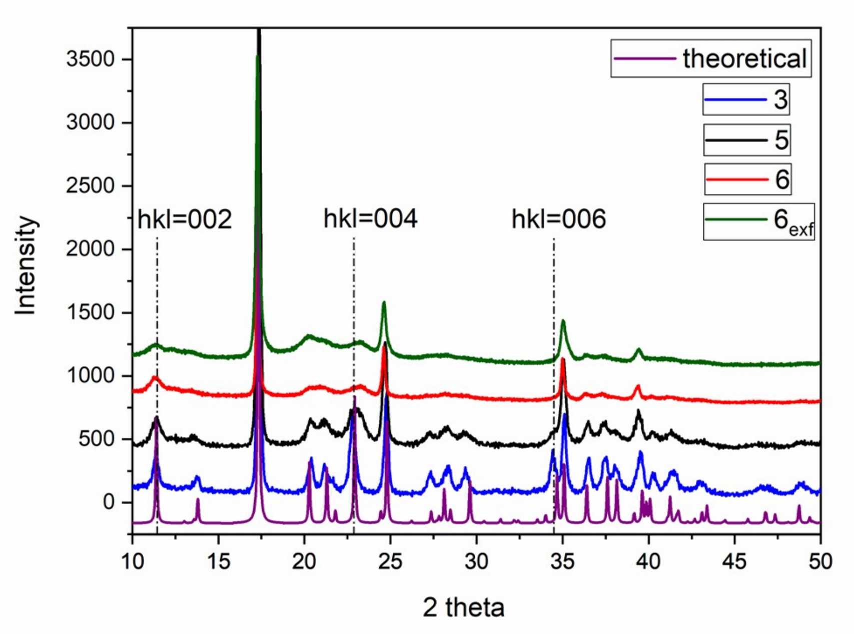

Fig. S9. X-ray powder diffraction patterns for compound **3** and nanoparticles **5**, **6** and **6$_{exf}$**. The theoretical p-xrd pattern of the bulk analogue is also presented for comparison reasons.[71]

UV-Vis spectra in ethanol

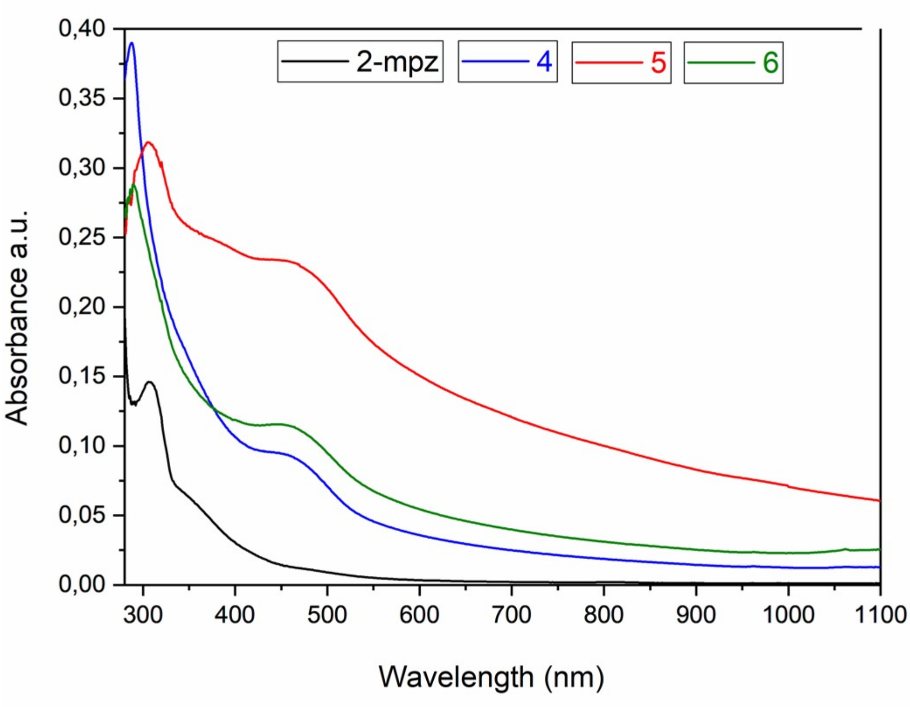

Fig. S10. UV-Vis spectra in ethanol for the ligand as well as nanoparticles **4**, **5** and **6**.

UV-Vis spectra in water

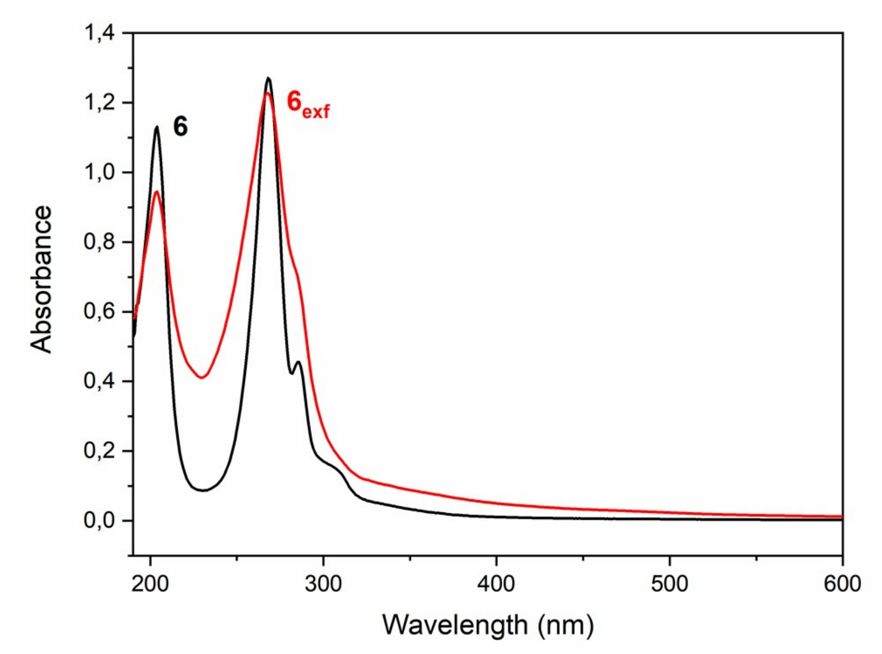

Fig. S11. UV-Vis spectra in water for nanoparticle **6** and the exfoliated species $\mathbf{6}_{\mathbf{exf}}$.

Aging effects / IR spectroscopy

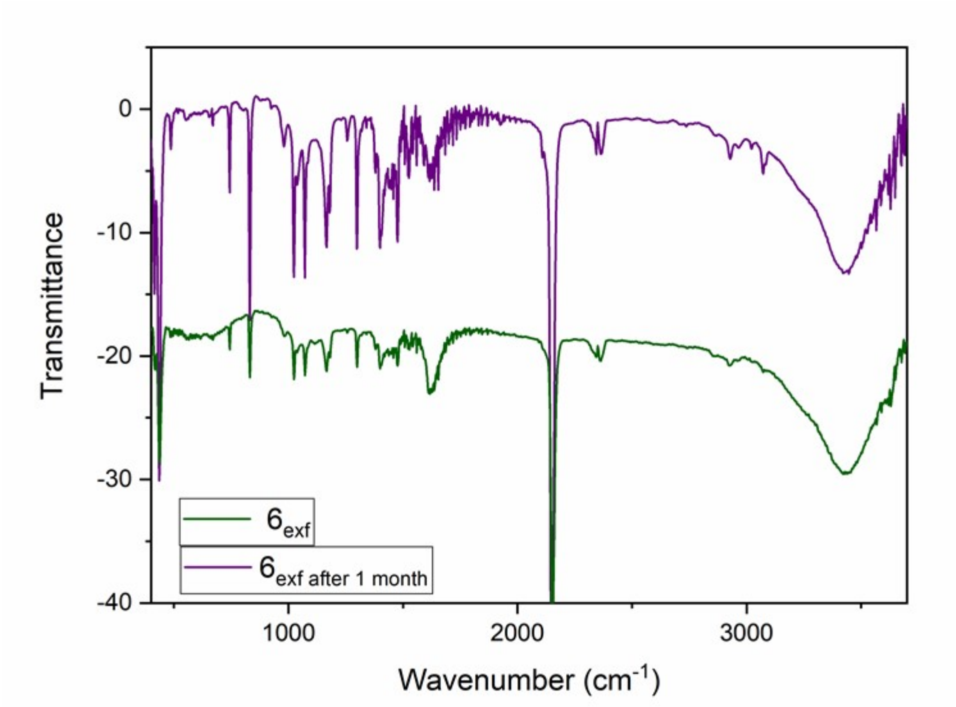

Fig. S12. Comparison of the IR spectra between nanoparticles $\mathbf{6_{exf}}$ and $\mathbf{6_{exf}}$ after 1 month.

Aging effects / Uv-Vis spectroscopy

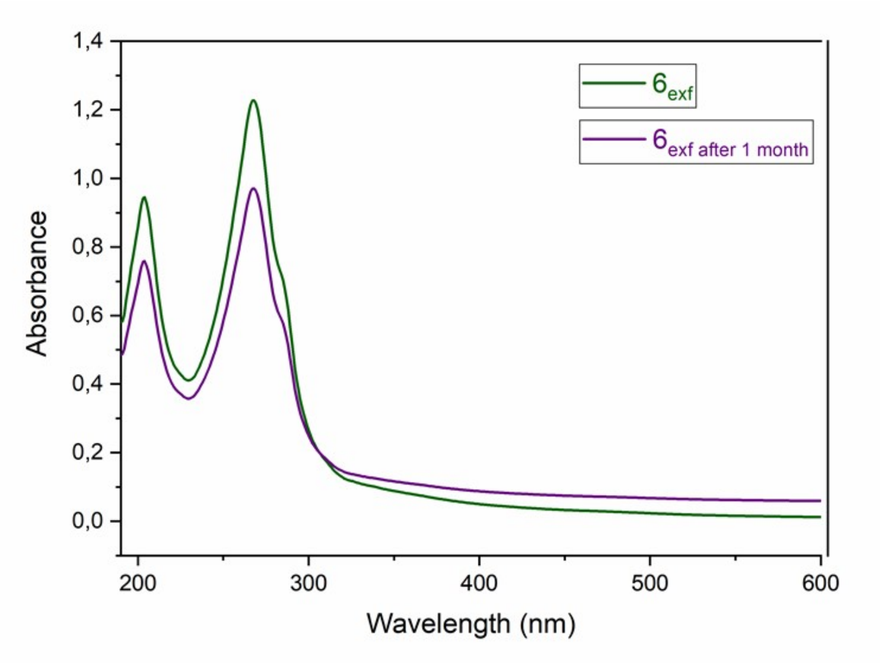

Fig. S13. Comparison of the UV-Vis spectra in water between nanoparticles $\mathbf{6}_{\mathbf{exf}}$ and $\mathbf{6}_{\mathbf{exf}}$ after 1 month.

Aging effects / pXRD

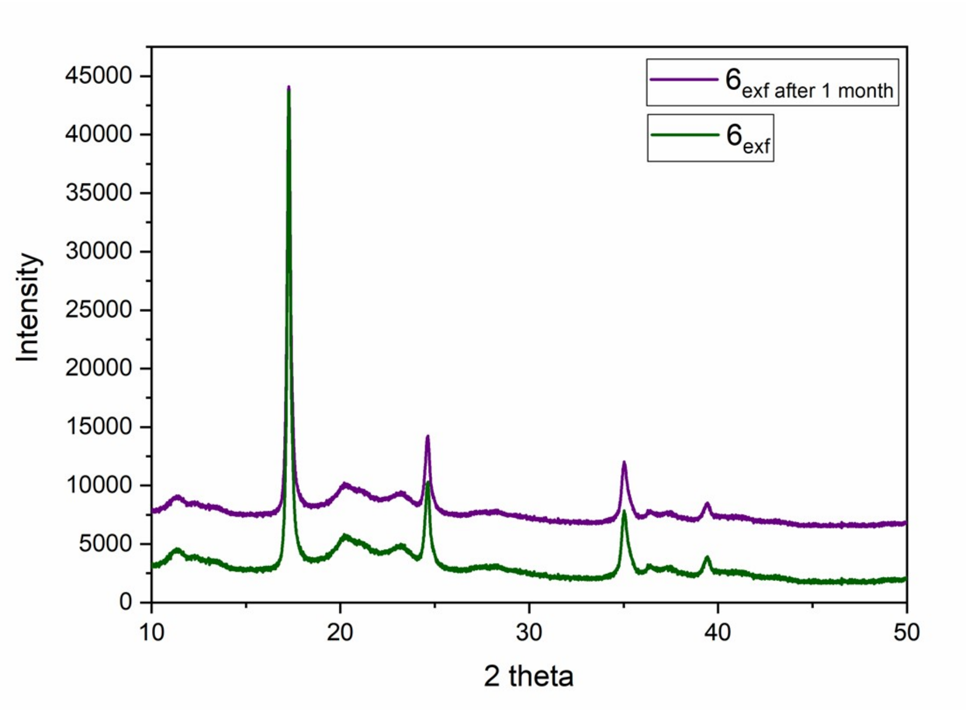

Fig. S14. Comparison of the X-ray powder diffraction patterns between nanoparticles **6**$_{exf}$ and **6**$_{exf}$ after 1 month.

Tyndall Effect

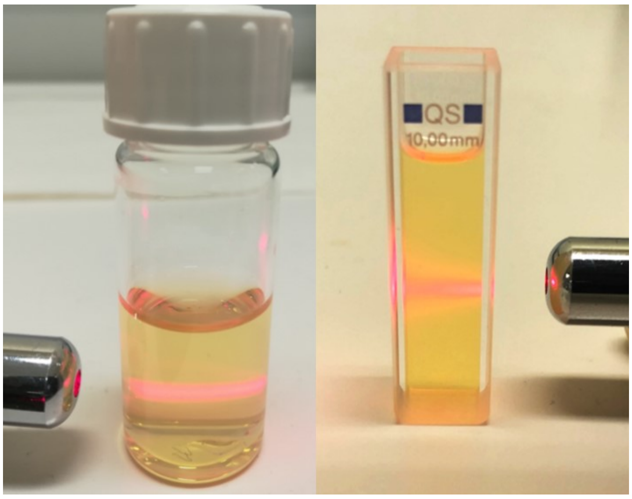

Fig. S15. The Tyndall Effect in colloidal dispersions of water (left) and acetone (right) of **6**$_{\mathbf{exf}}$.

DLS measurements and zeta potential

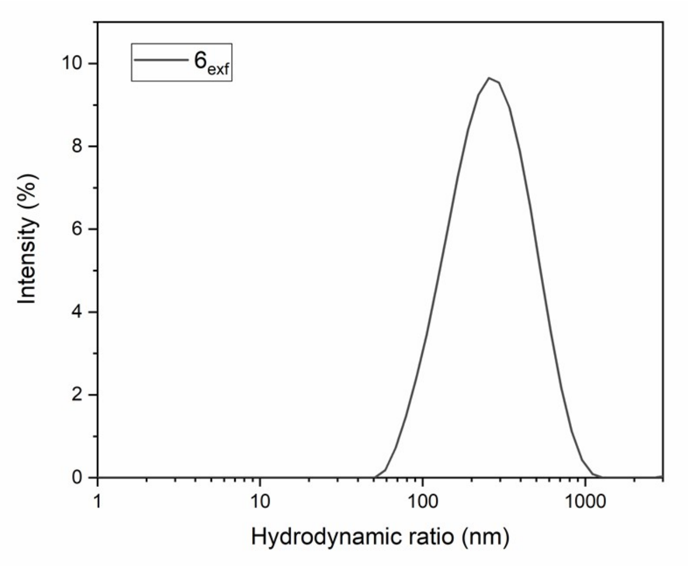

Fig. S16. DLS size distribution curve for $\mathbf{6_{exf}}$.

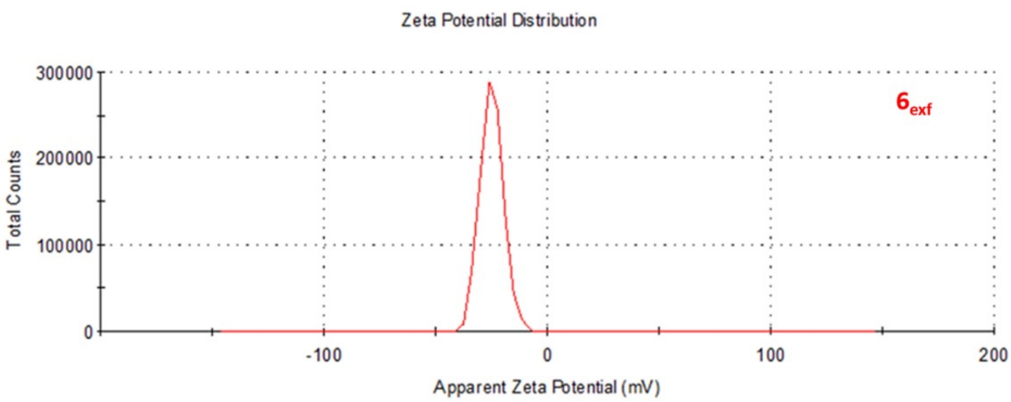

Fig. S17. Zeta potential distribution curve for 6_{exf}.

Thermal hysteresis and first derivatives

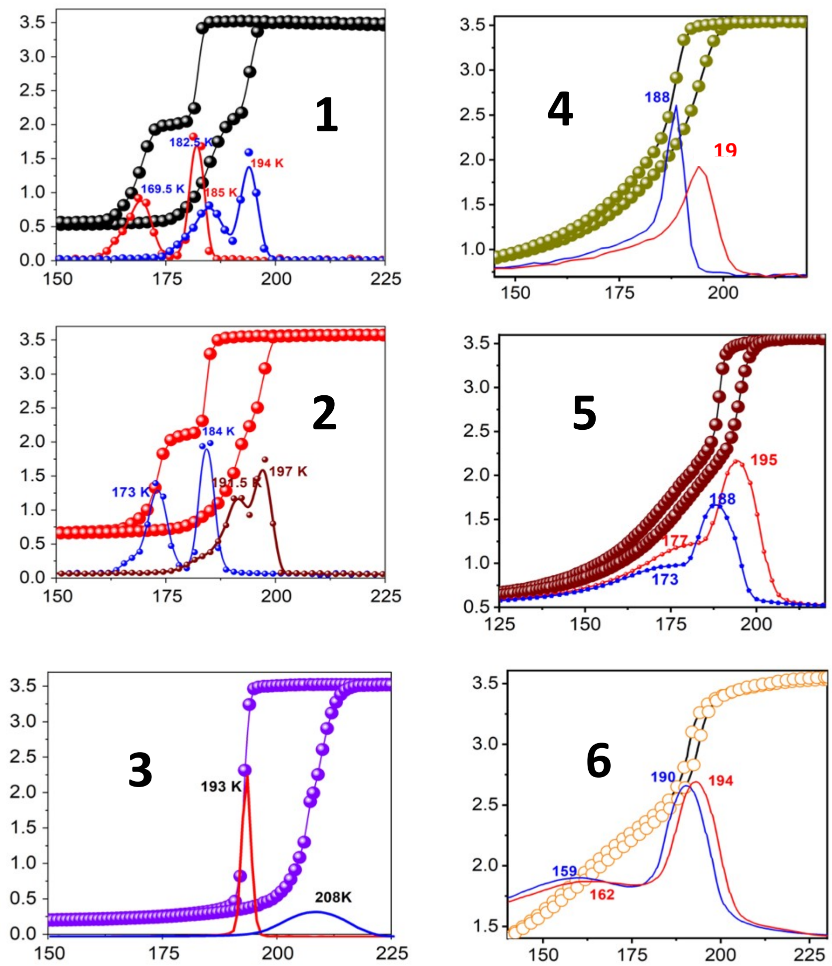

Fig. S18. First derivative plots (solid lines) of the magnetic susceptibility curves along with the experimental magnetic susceptibility (solid cycles) for **1** - **6**.

DSC measuremets of **4-6**

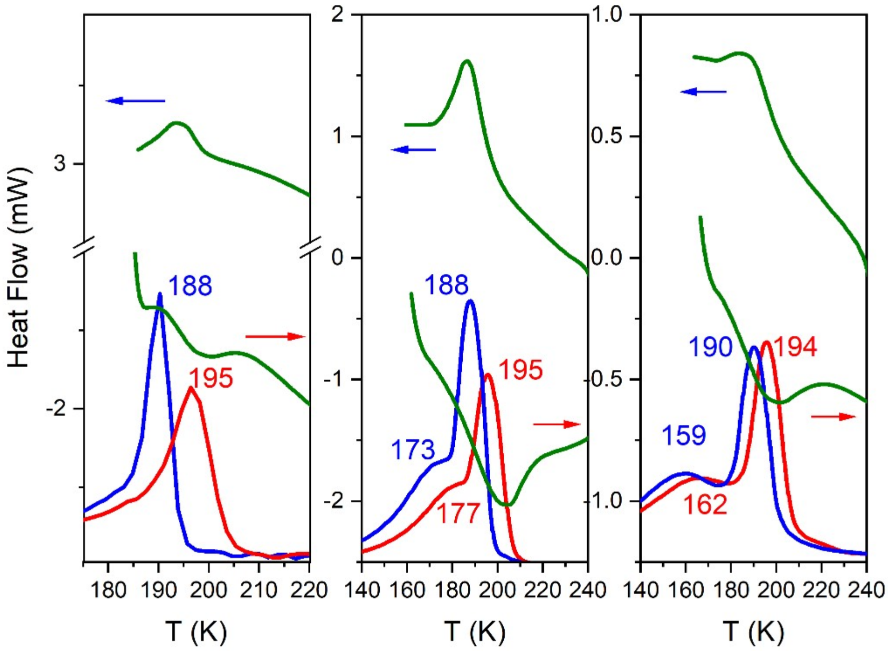

Fig. S19. Thermal dependence of the first derivatives (blue lines are for the cooling mode and red lines for the heating mode) of the $\chi_M T$ product and DSC analysis for nanoparticles **4**, **5** and **6** with scan rate 10 K min^{-1}.

Table S4. Experimental values of the critical temperatures for nanoparticles **4-6** and **6_{exf}** based on the first derivatives of the magnetic susceptibility curves and the DSC measurements.

	Magnetic Measurements		DSC measurements	
	Tc_1	**Tc_2**	**Tc_1**	**Tc_2**
4	188 K, 195 K	no	188 K, 197 K	no
5	188 K, 195 K	177 K, 173 K	188 K, 198 K	**no**
6	190 K, 194 K	159 K, 162 K	190 K, 197 K	**no**
6_{exf}	194 K, no	no	192 K, 189 K	**no**

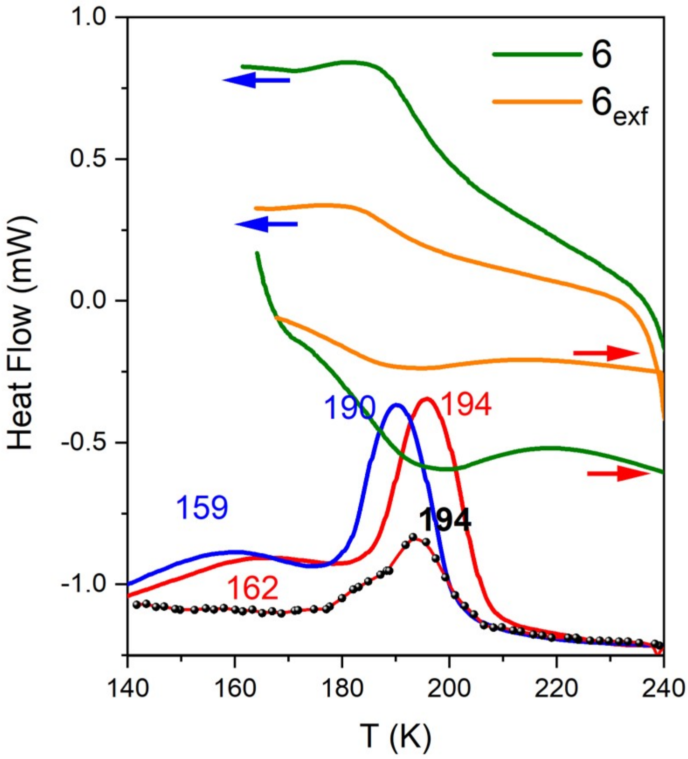

DSC measuremets of 6exf

Fig. S20. Thermal dependence of the first derivatives (blue line is for the cooling mode and red line for the heating mode of nanoparticle **6** while black spheres connected with red line is for nanoparticle **6exf)** of the $\chi_M T$ product and DSC analysis for nanoparticles **6** and $\mathbf{6_{exf}}$ with scan rate 10 K min^{-1}.